Hindawi
Shock and Vibration
Volume 2017, Article ID 9659425, 8 pages
https://doi.org/10.1155/2017/9659425

Research Article

Force Feedback Control Method of Active Tuned Mass Damper

Xiuli Wang[1,2] and Di Yun[1,2]

[1]*School of Civil Engineering, Jilin Jianzhu University, Changchun 130118, China*
[2]*Jilin Structure and Earthquake Resistance Technology Innovation Center, Changchun 130118, China*

Correspondence should be addressed to Xiuli Wang; wangxljz1976@163.com

Received 7 June 2017; Accepted 4 October 2017; Published 30 October 2017

Academic Editor: Enrico Zappino

Active tuned mass dampers as vibration-control devices are widely used in many fields for their good stability and effectiveness. To improve the performance of such dampers, a control method based on force feedback is proposed. The method offers several advantages such as high-precision control and low-performance requirements for the actuator, as well as not needing additional compensators. The force feedback control strategy was designed based on direct-velocity feedback. The effectiveness of the method was verified in a single-degree-of-freedom system, and factors such as damping effect, required active force, actuator stroke, and power consumption of the damper were analyzed. Finally, a simulation study was performed by configuring a main complex elastic-vibration-damping system. The results show that the method provides effective control over modal resonances of multiple orders of the system and improves its dynamics performance.

1. Introduction

A tuned mass damper (TMD) suppresses structural vibrations by improving the damping characteristics of the structure. The device has been successfully applied in fields including rail transportation [1], aviation [2], and aerospace [3] and structural [4] engineering. Compared with general passive TMDs, active TMDs (ATMDs) offer advantages such as small mass, good control, and broader potential in applications.

The control strategy of an ATMD is at the core of research in this technology. To date, the control methods that have been developed include pole configuration [5], state-parameter feedback [6], active damping [7], and delay feedback [8]. Among these methods, active damping is widely used because of its good stability and low energy consumption. Currently, active damping methods that are being pursued include advanced, positive-position-feedback (PPF), and direct-velocity-feedback controls. The advanced control uses a lead compensator, which improves the damping of all modes in a frequency band [9]. Direct velocity feedback involves direct feedback of the velocity signals at the measurement point. The principle and realization of this control method are relatively simple and hence have been adopted in many applications. Elliott et al. studied the maximum feedback gain for direct-velocity feedback when the actuator itself has greater damping and a natural frequency lower than the frequency of the main vibration-absorbing system. Elliott et al. developed a second-order compensator that acts as a general inertial actuator for a low-frequency, high-damping damper [7]. The PPF method uses a second-order compensator as controller, which has a relatively narrow vibration damping bandwidth and achieves better acceleration feedback. The PPF control method is adopted for the ATMD used in the Stratospheric Observatory for Infrared Astronomy developed by the US National Aeronautics and Space Administration and the German Aerospace Center [10]. Similar to the direct-velocity feedback, the PPF requires a compensator to improve the closed-loop control performance of the system.

All the control methods for ATMDs that are currently studied use for feedback kinematic parameter such as acceleration, velocity, and displacement, and the measurement of these parameters is performed mainly with acceleration sensors. Acceleration sensors are easy to use, but factors such as cost, large interference from environmental noise, drift during long-term use, and the need for recalibration limit their practical application to ATMDs. Compared with acceleration sensors, a force sensor has higher accuracy and low

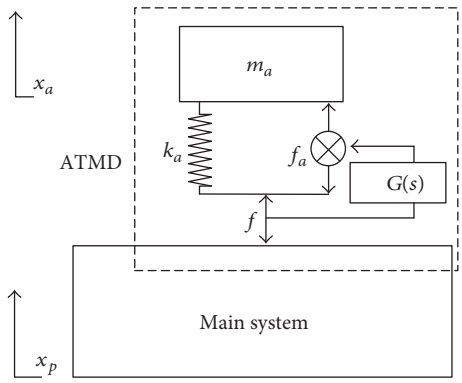

Figure 1: Schematic of the ATMD system.

noise interference and hence in practice is more suitable. This paper presents then an ATMD force feedback control method based on force sensors that takes advantages of good feedback stability and low noise interference. It reduces the performance requirements of the actuator via control-rate specifications as there is no need for compensators to be set. We assess control strategy designs, provide a parameter analysis, and conduct corresponding simulations.

2. ATMD Force Feedback Control Strategy

From the schematic of an ATMD-vibration damping system (Figure 1), the ATMD is mounted on the main system. It is modeled as a spring-mass unit, where m_a represents the mass of the block and k_a represents the spring stiffness. An active control force f_a is applied between the main system and the ATMD mass block. As a general actuator has less self-damping, the impact of damping is initially considered negligible.

The force f acting between the ATMD and the main system is measured in real time using a piezoelectric force sensor. This measured force is inputted to the controller $G(s)$ and used in calculating the system's active control force f_a. After passing through a power amplifier, it drives the voice-coil motor and thereby achieves vibration control.

The design of the controller $G(s)$ is the essential task of the study. Partial modeling of the ATMD system yields

$$\begin{aligned} f &= k\left(x_p - x_a\right) + f_a, \\ f &= m\ddot{x}_a, \end{aligned} \tag{1}$$

where x_a and x_p represent the vibration displacements of the ATMD mass block and main system, respectively. Applying a Laplace transformation to both (1) gives

$$\begin{aligned} F &= k\left(X_p - X_a\right) + F_a \\ F &= ms^2 X_a. \end{aligned} \tag{2}$$

Assuming that

$$F_a = G(s)\, F \tag{3}$$

then (2) becomes

$$F = k\left(X_p - X_a\right) + G(s)\, F \tag{4}$$

Combined with (4), we obtained

$$F = \frac{k}{1 + k/ms^2 - G(s)} X_p \tag{5}$$

For comparison, direct-velocity-feedback control would require

$$-F = -gsX_p, \tag{6}$$

where g represents the feedback gain and $-F$ is the force applied by the damper to the main system. Equating (5) and (6) yields expression

$$G(s) = 1 + \frac{k}{ms^2} - \frac{k}{gs}. \tag{7}$$

Under reparameterization,

$$G(s) = 1 + \frac{\omega_a^2}{s^2} - \mu\frac{\omega_a^2}{s} = \frac{s^2 - \mu s + \omega_a^2}{s^2}, \tag{8}$$

where $\omega_a^2 = k/m$ and $\mu = m\omega_a^2/g$. Equation (8) determines the force feedback control strategy of the ATMD. As $G(s)$ has a pole at $s = 0$ that affects the system stability, a nonzero pole needs to be established to improve the stability. Hence, the specific controller is assumed to adopt the form

$$N(s) = \frac{s^2 - \mu s + \omega_a^2}{s^2 + ps + q}. \tag{9}$$

To ensure that the impact on the system is small, the values of p and q should be relatively small.

The ATMD power consumption is also a factor that needs to be considered in the design. This is calculated from

$$W = \frac{1}{2}\mathrm{Real}\left(F_a{}^T \cdot V\right) + \frac{1}{2}\mathrm{Real}\left(-F_a{}^T \cdot V_p\right), \tag{10}$$

where V and V_p are the vibration velocities of the damper mass and main system, respectively. In general, V of the ATMD mass is much greater than V_p, so the second term in (10) can be ignored.

3. Simulation of the Single-Degree-of-Freedom System

To verify the method's effectiveness, a simulation study was conducted of a single-degree-of-freedom system model (Figure 2). The parameters used in the simulation are listed in Table 1.

The root locus curve is drawn for parameter μ using (9) for the closed-loop control system (Figure 3). As μ is inversely proportional to the control gain g, the direction of movement for g on the root locus is from zero to the pole. The system is stable as long as g is greater than 2278; the final state gives a damping ratio of 0.221. As g increases, the system's natural frequency changes; its maximum frequency is 45.06 Hz. Given factors such as stability and feasibility, the feedback gain g is set at 8000 in simulations.

Table 1: Simulation parameter settings.

System parameter	Values
Main system mass	100 kg
Natural frequency of main system	40 Hz
Damping ratio of main system	0.002
Damper mass	1 kg
Natural frequency of damper	40 Hz
Damping ratio of damper	0.001

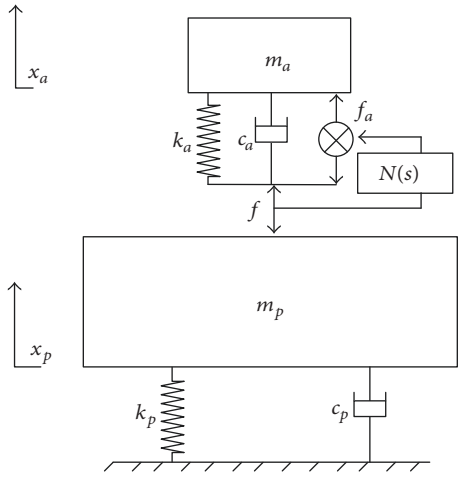

Figure 2: Schematic of the ATMD system.

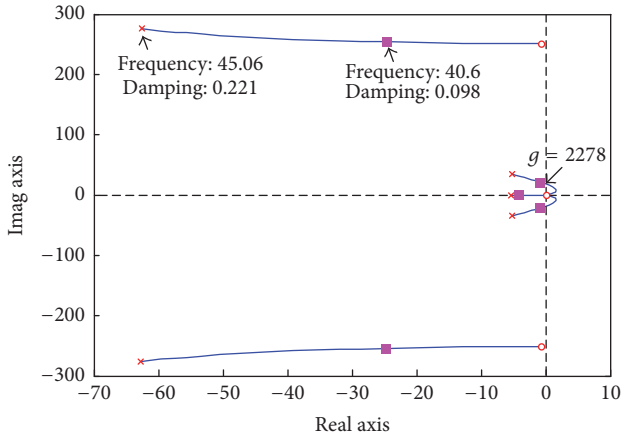

Figure 3: Closed-loop root locus diagram of the system.

3.1. Comparison of Damping Effect. First, the effectiveness of damping for the control method was analyzed. Figure 4 shows the damping curves for the ATMD with the natural frequency set at 30 Hz, 40 Hz, and 50 Hz in the main system. Mounting each different ATMD inhibits strongly the system's formant. From the phase diagram, a slow transition occurs on both sides of 90° resonance phase angle, indicating that after installing the ATMD damping of the system's resonance mode has been effective. Damping for the different absorbers was not significantly different, indicating that using force feedback control strategy is not affected by the natural

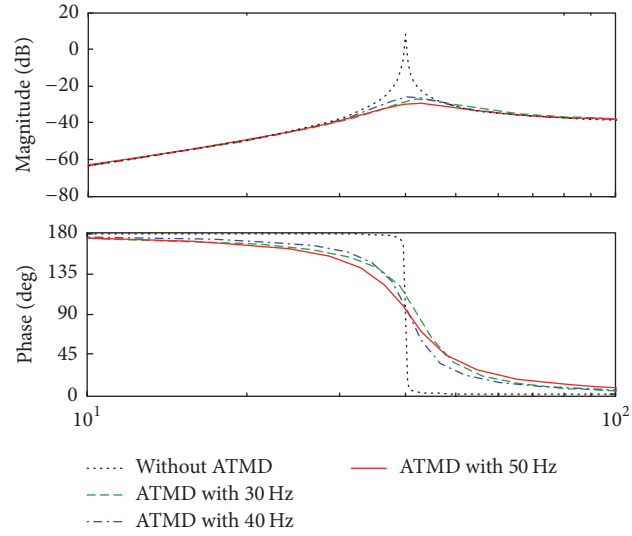

Figure 4: Vibration attenuation in the ATMDs with different frequencies.

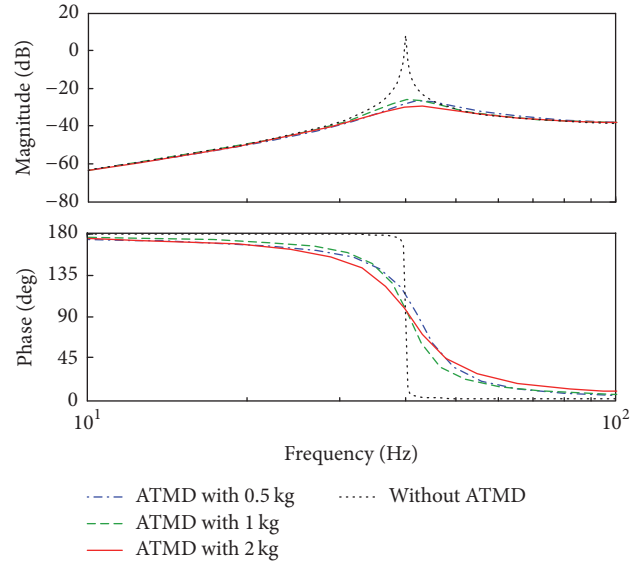

Figure 5: Vibration attenuation of ATMDs of different masses.

frequency of the ATMD itself. Hence there is no need to add compensators to counter the ATMD's own characteristic response.

Figure 5 shows a comparison of the ATMD damping when different natural frequencies are set by setting the mass to 0.5 kg, 1 kg, and 2 kg in the main system. The three ATMDs achieve better damping with the greater mass performing better than the other two. Nevertheless, the difference in damping by varying the mass is not obvious implying that the ATMD mass has little effect on the control strategy.

3.2. ATMD Active Force Analysis. As the output forces from the actual actuator have a certain range, which cannot be increased indefinitely, we need to analyze the demand of the force feedback control method in regard to these output

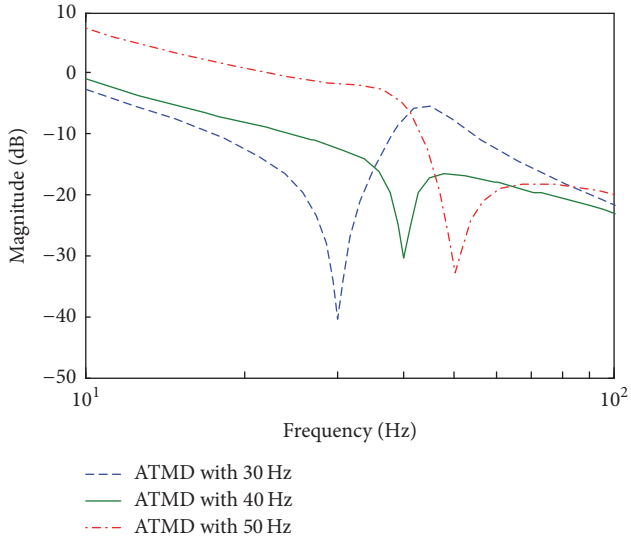

Figure 6: Required active force of ATMDs with different natural frequencies.

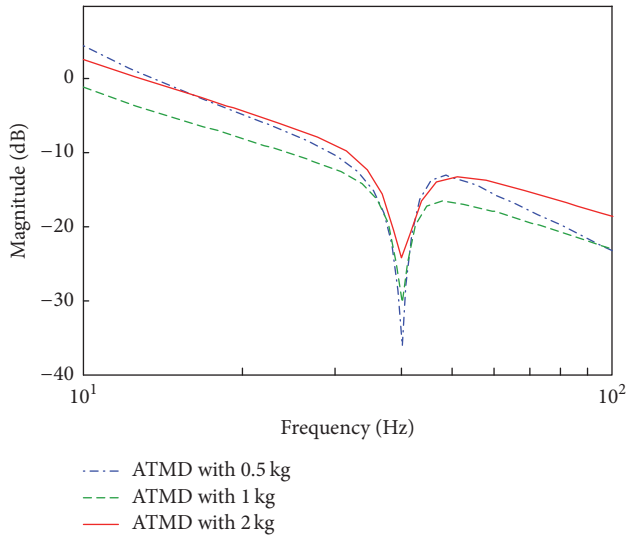

Figure 7: Needed active force of ATMDs of different mass.

forces. Figure 6 gives a comparison of the required active forces when the natural frequency of the ATMD was set to 30 Hz, 40 Hz, and 50 Hz. Each curve shows a high downward trend at low frequency and a low downward trend at high frequency. A very obvious valley appears at the natural frequency of the ATMD. The reason is that at resonance the structural part of the ATMD acts as an absorber of vibrational energy that suppresses the active force. Therefore, in practical applications, the natural frequency of the ATMD must be set at the main disturbance frequency of the system where the ATMD can effectively reduce the required active force. In comparing the three ATMDs, we see that in the low-frequency band a lower natural frequency for the ATMD elicits a smaller required active force because with higher frequencies and greater system rigidity a stronger active force is needed to overcome the spring force. The main active force required by each ATMD converges to the same value in the high-frequency band.

Figure 7 shows a comparison of the required active forces for three ATMDs of masses 0.5 kg, 1 kg, and 2 kg in main system. At the natural frequency of the ATMD, the greater its mass is, the greater the required active force is.

3.3. ATMD Actuator Stroke Analysis. The ATMD actuator stroke is also an important factor to consider in practical applications. Therefore, an analysis is necessary in regard to the influence of the force feedback control method on the ATMD actuator stroke. Figure 8 shows a comparison of the ATMD stroke for the different frequencies in the main system. At low frequency the stroke is long whereas at high frequency the stroke is short. The peak value of the stroke curve appears at the natural frequency (40 Hz) of the main system. A comparison of the three ATMDs shows that there is no real difference in stroke at 30 Hz and 50 Hz with 40 Hz being slightly smaller; the three ATMD strokes at the peak were not much different.

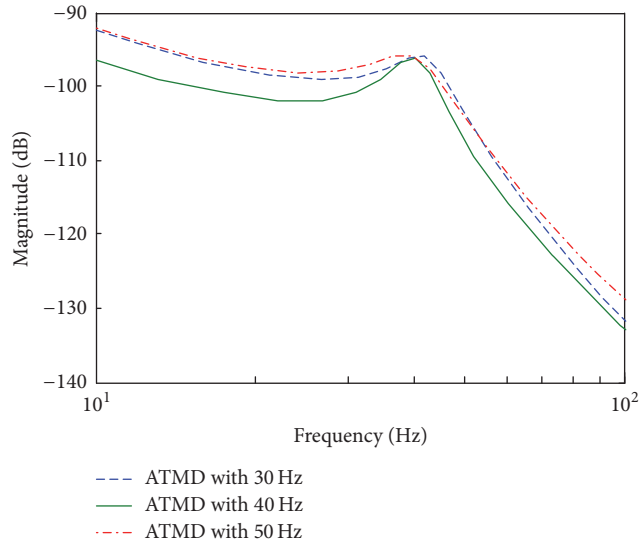

Figure 8: Stroke of the ATMDs for different natural frequencies.

Figure 9 shows a comparison of the stroke of ATMDs with mass of 0.5 kg, 1 kg, and 2 kg. The trend in each curve is basically the same, although clearly the larger mass yields smaller stroke.

3.4. Analysis of Power Consumption Required by the ATMD. Power consumption strongly reflects the nature of the stroke and active force. Figure 10 shows a comparison of the power consumption for the ATMDs when three different resonance frequencies were set in the system. Similar to the active force curve, each ATMD features a valley at its own natural frequency, indicating that the required power consumption under these conditions is minimal.

Figure 11 shows a similar comparison of the power consumption for three ATMDs but of different masses. The valleys appear at frequency 40 Hz of the ATMDs with power

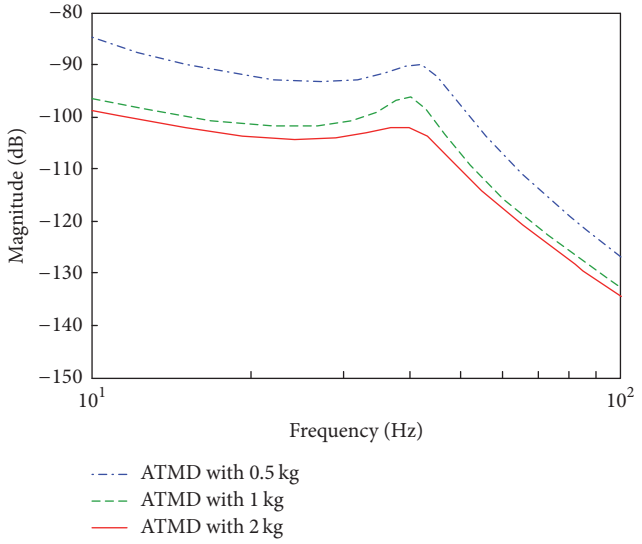

Figure 9: Stroke of the ATMDs for three different masses.

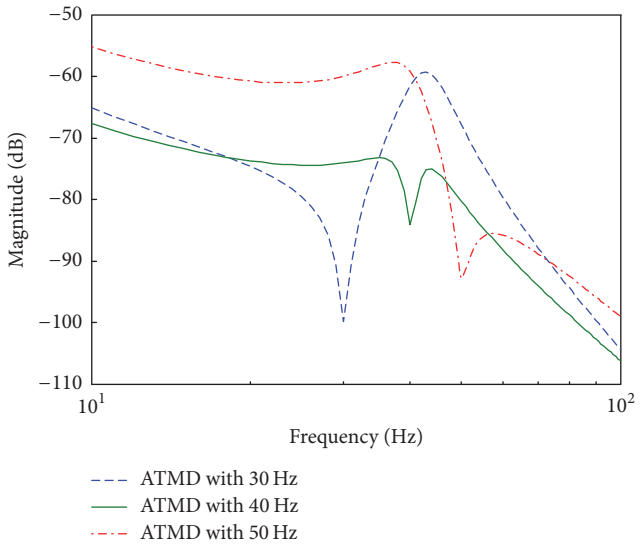

Figure 10: Power of the ATMDs with different natural frequencies.

consumption being basically the same. For other frequencies, the 0.5 kg ATMD incurs higher power consumption whereas those for the 1 kg and 2 kg ATMDs were not much different. Comparing the total active force and stroke, the curves indicate that the higher power consumption for the 0.5 kg ATMD is mainly due to its larger stroke.

4. Verification of Complex System

The practicality of the force feedback control method was verified using the single-degree-of-freedom main system described above, and further simulations were performed for a main complex system. The following methods can be used to simulate how ATMDs respond when used in conjunction with main complex systems.

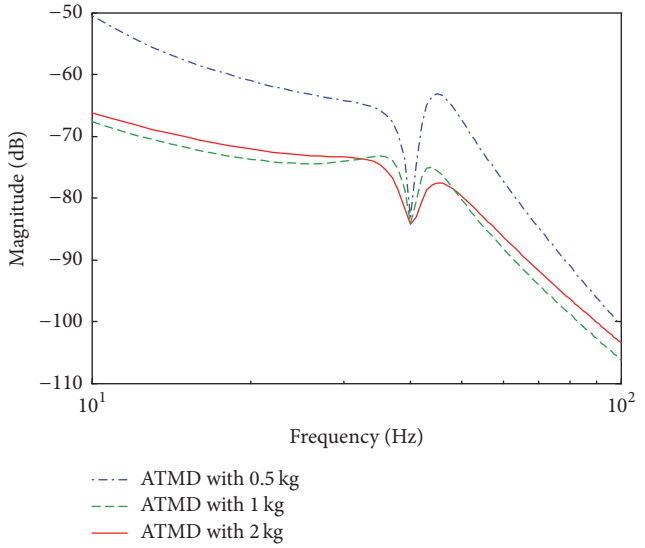

Figure 11: The power of the ATMDs with different mass.

First, the differential equation governing the dynamics of a complex system was established:

$$M\ddot{x}(t) + C\dot{x}(t) + Kx(t) = q(t), \tag{11}$$

where M is the mass matrix, C the damping matrix, and K the stiffness matrix. The Laplace transformation is applied to both sides to yield

$$\left(Ms^2 + Cs + K\right)X = Q, \tag{12}$$

where

$$X = \begin{bmatrix} X_1 \\ \cdots \\ X_q \\ X_a \\ X_b \end{bmatrix},$$

$$Q = \begin{bmatrix} 0 \\ \cdots \\ F \\ 0 \\ 0 \end{bmatrix},$$

$$M = \begin{bmatrix} m_{11} & \cdots & m_{1q} & m_{1a} & m_{1b} \\ \cdots & \cdots & \cdots & \cdots & \cdots \\ m_{q1} & \cdots & m_{qq} & m_{qa} & m_{qb} \\ m_{a1} & \cdots & m_{aq} & m_{aa} & m_{ab} \\ m_{b1} & \cdots & m_{bq} & m_{ba} & m_{bb} \end{bmatrix},$$

$$C = \begin{bmatrix} c_{11} & \cdots & c_{1q} & c_{1a} & c_{1b} \\ \cdots & \cdots & \cdots & \cdots & \cdots \\ c_{q1} & \cdots & c_{qq} & c_{qa} & c_{qb} \\ c_{a1} & \cdots & c_{aq} & c_{aa} & c_{ab} \\ c_{b1} & \cdots & c_{bq} & c_{ba} & c_{bb} \end{bmatrix},$$

$$K = \begin{bmatrix} k_{11} & \cdots & k_{1q} & k_{1a} & k_{1b} \\ \cdots & \cdots & \cdots & \cdots & \cdots \\ k_{q1} & \cdots & k_{q2} & k_{qa} & k_{qb} \\ k_{a1} & \cdots & k_{aq} & k_{aa} & k_{ab} \\ k_{b1} & \cdots & k_{bq} & k_{ba} & k_{bb} \end{bmatrix}. \tag{13}$$

For vector X, X_a and X_b are, respectively, the Laplace transforms of the vibration displacements at the ATMD and the ATMD installation points. The force feedback control strategy is written:

$$f_{\text{act}} = \frac{s^2 - \mu s + \omega_a^2}{s^2 + ps + q} m_a s^2 X_a, \tag{14}$$

where f_{act} is the active control force and X_a is the vibration displacement of the ATMD mass block. To simplify the analysis of intermediate variables, we may introduce

$$X_i = \frac{m_a s^2}{s^2 + ps + q} X_a \tag{15}$$

and write

$$f_{\text{act}} = \left(s^2 - \mu s + \omega_a^2\right) X_i \tag{16}$$

Based on (15) and (16), (12) is reexpressed as

$$\left(M' s^2 + C' s + K'\right) X' = Q', \tag{17}$$

where

$$X' = \begin{bmatrix} X_1 \\ \cdots \\ X_q \\ X_a \\ X_b \\ X_i \end{bmatrix},$$

$$Q' = \begin{bmatrix} 0 \\ \cdots \\ F \\ 0 \\ 0 \\ 0 \end{bmatrix},$$

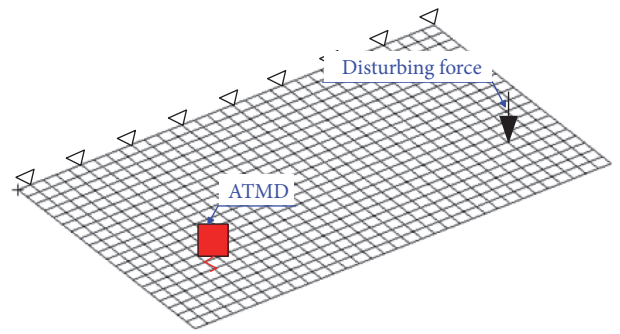

Figure 12: Model of the major structures of the damping system.

$$M' = \begin{bmatrix} m_{11} & \cdots & m_{1q} & m_{1a} & m_{1b} & 0 \\ \cdots & \cdots & \cdots & \cdots & \cdots & 0 \\ m_{q1} & \cdots & m_{qq} & m_{qa} & m_{qb} & 0 \\ m_{a1} & \cdots & m_{aq} & m_{aa} & m_{ab} & -1 \\ m_{b1} & \cdots & m_{bq} & m_{ba} & m_{bb} & 1 \\ 0 & 0 & 0 & -m_a & 0 & 1 \end{bmatrix},$$

$$C' = \begin{bmatrix} c_{11} & \cdots & c_{1q} & c_{1a} & c_{1b} & 0 \\ \cdots & \cdots & \cdots & \cdots & \cdots & 0 \\ c_{q1} & \cdots & c_{qq} & c_{qa} & c_{qb} & 0 \\ c_{a1} & \cdots & c_{aq} & c_{aa} & c_{ab} & \mu \\ c_{b1} & \cdots & c_{bq} & c_{ba} & c_{bb} & -\mu \\ 0 & 0 & 0 & 0 & 0 & p \end{bmatrix},$$

$$K' = \begin{bmatrix} k_{11} & \cdots & k_{1q} & k_{1a} & k_{1b} & 0 \\ \cdots & \cdots & \cdots & \cdots & \cdots & 0 \\ k_{q1} & \cdots & k_{q2} & k_{qa} & k_{qb} & 0 \\ k_{a1} & \cdots & k_{aq} & k_{aa} & k_{ab} & -\omega_a^2 \\ k_{b1} & \cdots & k_{bq} & k_{ba} & k_{bb} & \omega_a^2 \\ 0 & 0 & 0 & 0 & 0 & q \end{bmatrix}. \tag{18}$$

The simulation of the main complex system can be completed in accordance with (17).

In this study, a supported plane clamped on one side was used as an elastic-vibration-damping system (see Figure 12). An ATMD was installed in one corner of the plane and a perturbative stimulus was applied at the corresponding opposing corner. The material of the elastic plane was aluminum alloy with modulus 70 GPa, density 2800 kg/m^3, size 1.65 m × 1 m × 0.03 m, and total mass 138.6 kg. The mass of the vibration absorber was 1 kg, and the feedback gain g was 8000.

First, the dynamics characteristics of the main system were analyzed and the finite element method was used to calculate the natural frequency and the vibration modes of the elastic plane up to fourth order (see Figure 13).

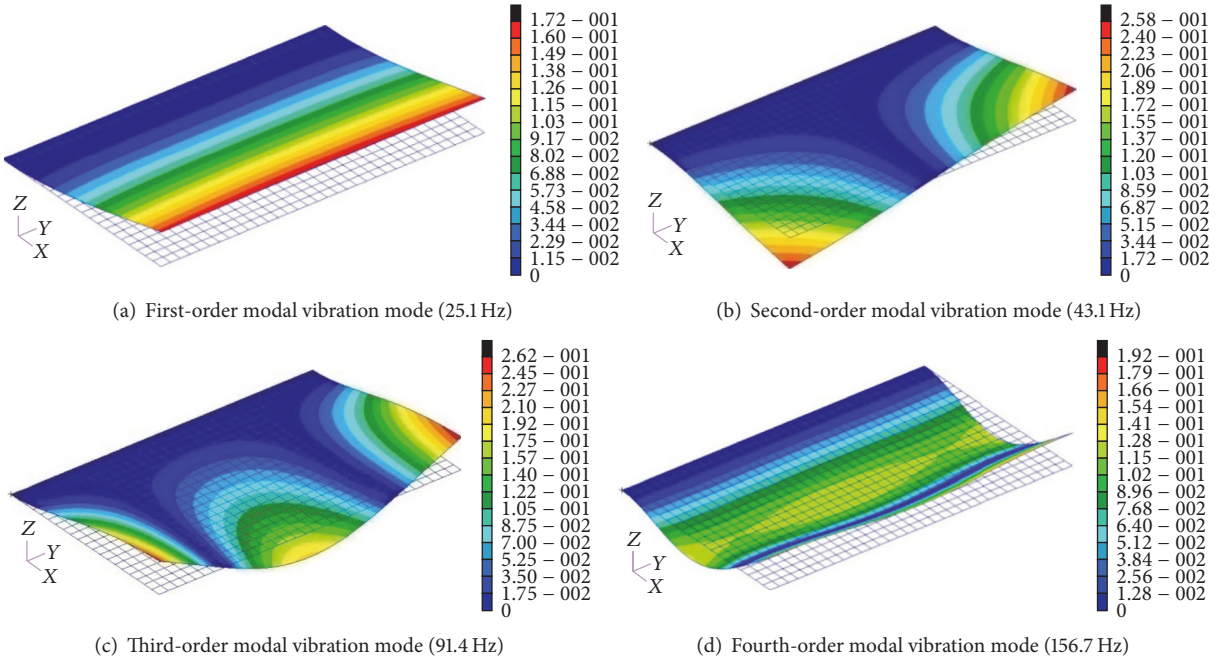

(a) First-order modal vibration mode (25.1 Hz)

(b) Second-order modal vibration mode (43.1 Hz)

(c) Third-order modal vibration mode (91.4 Hz)

(d) Fourth-order modal vibration mode (156.7 Hz)

Figure 13: Mode shapes of an elastic plane.

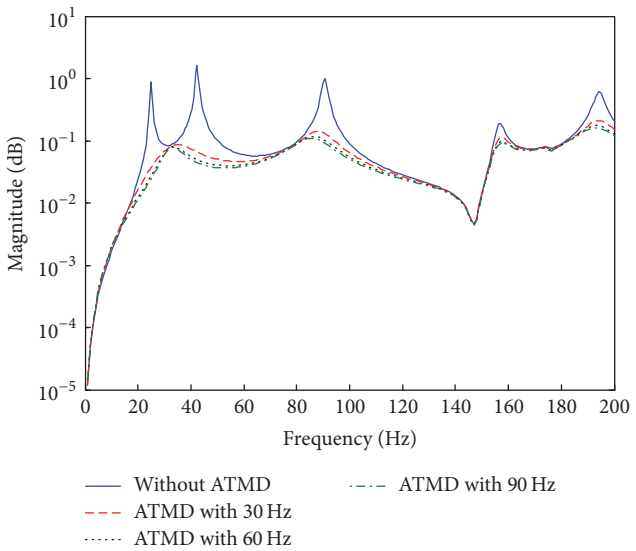

Figure 14: Vibration attenuation effect of the ATMD.

Figure 14 shows the transfer function curve of the system after an ATMD has been mounted. Without the absorber the transfer function of system (blue solid line) has a total of five peaks that correspond to the system's natural frequencies for the first five orders. As the damping of structure was small, the peaks are high and sharp. With ATMDs of frequencies 30 Hz, 60 Hz, and 90 Hz, the transfer functions of the system exhibit resonance peaks that are significantly attenuated. Of the five peaks, the attenuation of the fourth-order peak was relatively small as the ATMD is close to the nodal line for the resonance mode. A comparison between the three ATMDs shows no significant difference in vibrational effect. These results indicate that the force feedback control strategy is reliable in damping this main complex system and is not affected by the dynamics characteristics of the ATMD.

5. Conclusions

This paper presented a force feedback control method for ATMD. The results showed that this method can be used to achieve good vibration suppression. Compared with kinematic parameter feedback control, this method has the advantage of high-precision control and low dependence on actuator performance. Comparisons were given of control effects, stroke of actuator, required active force, and power consumption for various parameter values of the ATMD such as natural frequency and mass. The results showed that setting the natural frequency of ATMD at the vibration frequency of the main system offers benefits such as low power consumption and small stroke. In a simulation study, the calculation method was applied to a main complex system configured as an elastic planar structure. The results showed that the control strategy is able to control the multiordered modal vibration of this system and provides effective damping.

Conflicts of Interest

The authors declare that they have no conflicts of interest.

Acknowledgments

This work was supported by the National Natural Science Foundation of China under Grant no. 51308254.

References

[1] H. P. Liu, T. X. Wu, and Z. G. Li, "Theoretical modelling and effectiveness study of rail vibration absorber for noise control," *Journal of Sound and Vibration*, vol. 323, no. 3-5, pp. 594–608, 2009.

[2] O. A. Bauchau, J. Rodriguez, and S.-Y. Chen, "Modeling the bifilar pendulum using nonlinear, flexible multibody dynamics," *Journal of the American Helicopter Society*, vol. 48, no. 1, pp. 53–62, 2003.

[3] G. Ahmadi, J. F. Ellison, C. M. Grodsinsky, G. L. Anderson, and D. C. Lagoudas, "Vibration control of equipment aboard spacecraft," in *Proceedings of the Symposium on Active Materials and Smart Structures: Society of Engineering Science 31st Annual Meeting*, pp. 80–92.

[4] S. Nagarajaiah and E. Sonmez, "Structures with semiactive variable stiffness single/multiple tuned mass dampers," *Journal of Structural Engineering*, vol. 133, no. 1, pp. 67–77, 2007.

[5] K. Y. Lee, "Eigenvalue Estimation Using Linearly Dependent Eigenfunctions," *Journal of vibration and acoustics*, vol. 122, pp. 464–469, 2000.

[6] S. Chatterjee, "Optimal active absorber with internal state feedback for controlling resonant and transient vibration," *Journal of Sound and Vibration*, vol. 329, no. 26, pp. 5397–5414, 2010.

[7] S. J. Elliott, J. Rohlfing, and P. Gardonio, "Multifunctional design of inertially-actuated velocity feedback controllers," *The Journal of the Acoustical Society of America*, vol. 131, no. 2, pp. 1150–1157, 2012.

[8] J. Das and A. K. Mallik, "Control of friction driven oscillation by time-delayed state feedback," *Journal of Sound and Vibration*, vol. 297, no. 3-5, pp. 578–594, 2006.

[9] A. Preumont, *Vibration Control of Active Structures*, vol. 179 of *Solid Mechanics and its Applications*, Springer, Berlin, Germany, 3rd edition, 2011.

[10] P. J. Keas, "Active damping of the SOFIA telescope assembly," *SPIE*, 2012.